

Quantum simulation of the microscopic to macroscopic crossover using superconducting quantum impurities

Amir Burshtein^{1,*} and Moshe Goldstein¹

¹*Raymond and Beverly Sackler School of Physics and Astronomy, Tel Aviv University, Tel Aviv 6997801, Israel*

Despite being a pillar of quantum mechanics, little attention has been paid to the onset of the Fermi golden rule as a discrete microscopic bath of modes approaches the macroscopic thermodynamic limit and forms a continuum. Motivated by recent experiments in circuit quantum electrodynamics, we tackle this question through the lens of single-photon decay in a finite transmission line coupled to a qubit (“quantum impurity”). We consider a single-photon state, coupled via the nonlinear impurity to several baths formed by multi-photon states with different number of photons, which are inherently discrete due to the finite length of the line. We focus on the late-time dynamics of the single-photon, and uncover the conditions under which the photon decoherence rate approaches the decay rate predicted by the Fermi golden rule. We show that it is necessary to keep a small but finite escape rate (unrelated to the impurity) for each single-photon mode to obtain a finite long-time inelastic decay rate. We analyze the contribution of the baths formed by many-body states with different number of photons, and illustrate how the decay rate induced by some bath of n photon states is enhanced by the presence of other baths of $m \neq n$ photon states, highlighting the contribution of cascade photon decay processes. Our formalism could be used to analyze recent experiments in superconducting circuits.

I. INTRODUCTION

Living up to the second part of its name, the Fermi golden rule (FGR) has been an essential element in the quantum theorist’s toolbox for nearly a century [1, 2]. As the FGR describes the decay of a quantum state into a macroscopic bath formed by a continuum of modes, it is natural to inquire about what happens when the bath becomes discrete. An immediate consequence of a discrete microscopic bath is the presence of periodic revival processes leading to deviations from exponential decay, which have been long reported theoretically [3–6], and later also experimentally, in nuclear decay [7], light-matter interaction [8, 9], and circuit quantum acoustodynamics [10]. However, a closely-related question has been addressed directly only recently [11] — how does the FGR emerge as the bath approaches the thermodynamic limit? Important motivations to this question have been studies of Fock-space localization [12] and many-body localization [13–15], which monitor the dynamics of some initial quantum state in a large interacting system, as well as works on thermalization in Floquet systems [16, 17], weak breaking of integrability and the onset of chaos [18–20], and quantum scars [21].

Experimentally, the process of approaching the thermodynamic limit could be directly realized in quantum simulators. A particularly convenient arena is provided by superconducting circuits, which allow for natural implementation of quantum impurity models, comprised of a Josephson array coupled to some nonlinearity imposed by a qubit. It was demonstrated that a single-photon propagating in the Josephson array could decay into multi-photon states with a high probability [22], due

to superstrong coupling between the Josephson array and the qubit [23, 24], and that the decay rates of those single-photons could be used as experimental and theoretical probes that elucidate the dynamics of the impurity [25–35]. While the Josephson arrays are very long and support a large number ($N \sim 10^4$) of single-photon states, they are inevitably finite, such that the photon spectrum is discrete rather than continuous. Indeed, Ref. [36] demonstrated that shortening the transmission line gives rise to avoided-crossings in the single-photon spectroscopy picture, due to level repulsions between the single-photon state and the discrete set of many-photon states. The mode spacing of n -photon states scales as $\Delta_n \sim \ell^{-n}$, where ℓ is the length of the Josephson array, and could be tuned to investigate the finite-size effects; relatedly, Ref. [37] demonstrated how the finite length of the array could be used to tailor the decay of a single-photon into a specific outgoing multi-photon state.

With experiments already exploring the effects of the finite length of the array, a theoretical analysis is in demand. Some work has already been performed; finite-size effects in circuit quantum electrodynamics were studied [38] in the context of the Schmid-Bulgadaev quantum phase transition [39, 40] and dual Shapiro steps [41]. More specifically, in the context of single-photon scattering, a phenomenological theory was proposed in Ref. [42] to reproduce the spectroscopy probed in Ref. [36]. Yet, the decay rates of the single-photons were not addressed, nor was the thermodynamic limit of a semi-infinite Josephson array.

In this work, we show how the FGR emerges in the inelastic scattering of single-photons off an impurity in a finite Josephson array. We consider an interacting model of a (nearly) quadratic bosonic transmission line, supporting photon eigenstates, terminated by a nonlinear impurity, depicted in Fig. 1(d). The photons are coupled to one another via wave-mixing terms provided by the im-

* burshtein2@mail.tau.ac.il

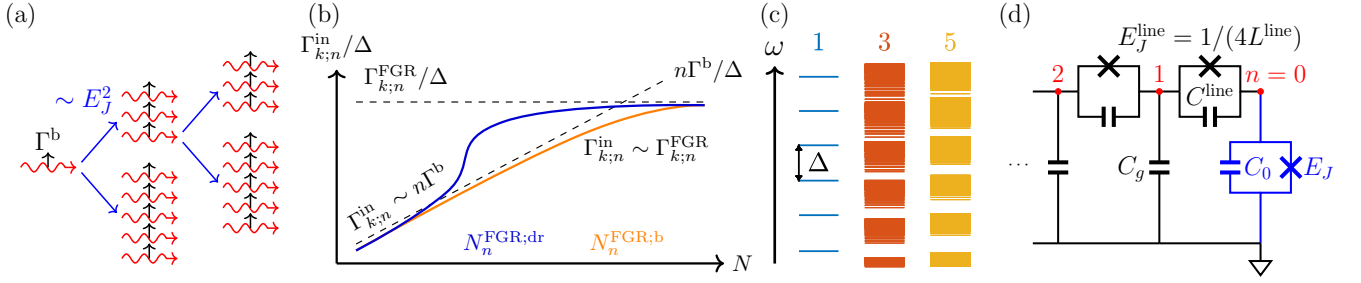


Figure 1. (a) Each photon is coupled to multiple many-body states via the impurity, and may also decay into the environment with a rate Γ^b . (b) Sketch of the main result, displaying the decay rate $\Gamma_{k;n}^{in}$ of some mode k induced by a bath of n -photon states with (blue) and without (orange) the dressing due to cascade decay processes into lower-frequency modes, as a function of the system size N . The rates are scaled by the single-photon mode spacing, $\Delta \sim 1/N$. At small N , $\Gamma_{k;n}^{in}$ is bounded by the bare broadening of the bath modes, $n\Gamma^b$. The decay rate approaches the rate predicted by the FGR, $\Gamma_{k;n}^{FGR}$, at large enough N , where $\Gamma_{k;n}^{FGR} < n\Gamma^b$. The dressing induced by the baths of $m \neq n$ -photon states reduces the crossover scale for the array size, $N_n^{FGR;dr}$ as compared to the scale $N_n^{FGR;b}$ in their absence, and allows for $\Gamma_{k;n}^{in} > n\Gamma^b$ in the crossover region. (c) Energies of 1-, 3-, and 5-photon states. The multi-photon levels are spread out by disorder and the curvature of the dispersion relation. (d) Quantum impurity model implemented by a Josephson array terminated with a Cooper-pair box.

purity, such that each single-photon state is coupled to many multi-photon states; states with different photon numbers thus behave as different baths. We focus on the late-time behavior of the survival probability of the initial state, and show that, if the array size is finite, one must keep a finite escape rate (unrelated to the impurity) of the single-photon states, unrelated to the nonlinearities in the impurity, to obtain a finite long-time inelastic rate. We uncover the conditions under which the inelastic decay rate induced by an n -photon bath approaches the rate predicted by the FGR for the corresponding infinite system, at large enough mode frequencies and array sizes. Applying a self-consistent approach, we show that the crossover of the n -photon bath into the thermodynamic regime, where its induced decay rate is given by the FGR, is accelerated by the presence of baths of $m \neq n$ -photon states, thanks to cascade processes depicted in Fig. 1(a). We further show that, in the crossover region of the n -photon bath, the $m \neq n$ -photon baths [see Fig. 1(c)] enhance the decay rate into the n -photon bath, allowing for values which would not have been possible in their absence. Our main results are sketched in Fig. 1(b), demonstrating the crossover of the n -photon bath rate from the microscopic regime, where it is dominated by the external decoherence rate of the single-photon states, into the macroscopic regime, where it approaches the FGR rate. Fig. 1(b) further illustrates the importance of the cascade decay processes, which enhance the n -photon bath rate in the crossover region and accelerate the convergence to the thermodynamic limit.

In this work we consider a Cooper-pair box impurity, where many multi-photon baths provide significant contributions to the total decay rate. Yet, our formalism could be easily adapted to explicitly address the finite-size effects on the decay rate of single-photons scattering off any type of impurity, and in particular could be used to analyze the experiment in Ref. [36], which con-

sidered a fluxonium impurity [43], and also applies to nonlinearities induced by weak bulk perturbations [44–47]. Similarly, we could also use our results to evaluate decoherence times of qubits coupled to a finite multimode resonator, which could be useful for quantum information processing applications.

The rest of the paper is organized as follows. In Section II, we discuss an exactly-solvable quadratic toy model of a resonant level coupled to an equidistant discrete bath. Though cascade decay processes are absent in this case, it nevertheless can teach us about some of the relevant effects. In particular, we show that an external broadening of the bath modes must be introduced to get a finite decay rate of the resonant level in the long-time limit, and find the conditions under which the decay rate approaches the FGR value. Then, in Section III, we consider the interacting model of a Josephson array coupled to a Cooper-pair box. We find the propagators of the single-photon modes by applying a self-consistent approach, which accounts for cascade processes into low-frequency modes. We calculate the FGR rates induced by each bath of $2n+1$ -photon states, and evaluate numerically the decay rates at finite array size, demonstrating the conditions for the microscopic to macroscopic crossover. We conclude in Section IV. The technical details of the evaluation of the FGR decay rates of the baths are relegated to Appendix A, and details regarding the numerical evaluation of the decay rates of the interacting system are discussed in Appendix B.

II. TOY MODEL — RESONANT LEVEL COUPLED TO AN EQUISPACED BATH

In this Section we consider a quadratic model, which cannot have cascade decay processes, yet can inform us some useful lessons. We study the Hamiltonian of the

resonant level model,

$$\mathcal{H} = \frac{\epsilon_d}{2} d^\dagger d + \sum_n \epsilon_n a_n^\dagger a_n + \sum_n (g_n d a_n^\dagger + g_n^* d^\dagger a_n), \quad (1)$$

where d, a_n are annihilation operators (either fermionic or bosonic) of the resonant level at ϵ_d and the bath modes at ϵ_n , respectively, and g_n are the coupling coefficients. Our goal is to obtain the decay rate Γ of the resonant level, determined from the late-time behavior of the survival probability, $\mathcal{P}_d(t) = |\langle d(t) d^\dagger(0) \rangle|^2 \sim e^{-\Gamma t}$ as $t \rightarrow \infty$. The survival probability can be extracted from the time-ordered propagator of the resonant mode, $\mathcal{P}_d(t) = |G_d(t)|^2$, where $G_d(t) = -i \langle \mathcal{T} d(t) d^\dagger(0) \rangle$, and \mathcal{T} stands for time-ordering. We calculate expectation values with respect to the vacuum state $|0\rangle$ which is annihilated by d, a_n (that is, $d|0\rangle = a_n|0\rangle = 0$), though generalization to expectation values in general excited states is straightforward. Since the toy model in Eq. (1) is quadratic, an exact solution for the time-ordered propagator is readily available in the frequency domain,

$$G_d(\omega) = -i \int_{-\infty}^{\infty} dt e^{i\omega t} \langle \mathcal{T} d(t) d^\dagger(0) \rangle = \frac{1}{\omega - \epsilon_d - \Sigma_d(\omega)}, \quad (2)$$

where $\Sigma_d(\omega) = \sum_n |g_n|^2 / (\omega - \epsilon_n)$ is the spectral function of the bath. From the inverse Fourier transform of $G_d(\omega)$, we find

$$\mathcal{P}_d(t) = \left| \int_{-\infty}^{\infty} \frac{d\omega}{2\pi} \frac{e^{-i\omega t}}{\omega - \epsilon_d - \Sigma_d(\omega)} \right|^2 = \left| \sum_{z_p} r_p e^{-iz_p t} \right|^2, \quad (3)$$

where z_p are solutions to $z - \epsilon_d - \Sigma_d(z) = 0$ with $\text{Im} z_p < 0$, and $r_p = \text{Res}_{z=z_p} 1 / (z - \epsilon_d - \Sigma_d(z))$. At $t \rightarrow \infty$, the survival probability is dominated by the pole with the smallest negative imaginary part (in absolute value), such that $\Gamma = -2 \min_{z_p} |\text{Im} z_p|$.

First, consider the textbook example of a bath composed of a continuum of modes with a constant density of states ν , spread across a bandwidth $2D$, and with a uniform coupling g . The Hamiltonian reads

$$\begin{aligned} \mathcal{H} = & \frac{\epsilon_d}{2} d^\dagger d + \nu \int_{-D}^D d\varepsilon a^\dagger(\varepsilon) a(\varepsilon) \\ & + \nu g \int_{-D}^D d\varepsilon (d a^\dagger(\varepsilon) + d^\dagger a(\varepsilon)), \end{aligned} \quad (4)$$

and the spectral function of the bath in the complex plane is given by

$$\begin{aligned} \Sigma_d(z = \omega + i\chi) &= \nu |g|^2 \lim_{\eta \rightarrow 0^+} \log \frac{z + D + i\eta}{z - D + i\eta} \\ &= \nu |g|^2 \log \left(-\frac{D^2 - \omega^2 - \chi^2 + 2i\chi D}{(\omega - D)^2 + \chi^2} \right). \end{aligned} \quad (5)$$

Taking the limit of a large bandwidth, $D \gg \nu |g|^2$ and $D \gg \epsilon_d$, we find that $z = \epsilon_d - i\pi\nu |g|^2$ is a solution to

$z - \epsilon_d - \Sigma_d(z) = 0$, up to corrections of order $\nu |g|^2 / D$ and ϵ_d / D , and we recover the textbook result, $\Gamma = \Gamma_{\text{FGR}} = -2 \text{Im} \Sigma_d(\omega = \epsilon_d) = 2\pi\nu |g|^2$.

Let us now we consider a discrete bath of uniformly-coupled ($g_n = g$), evenly-spaced modes, $\epsilon_n = \epsilon_d + \delta_{\min} + n\Delta$, where $n \in \mathbb{Z}$, Δ is the mode spacing, and $\delta_{\min} \in [-\Delta/2, \Delta/2]$ is the distance from the resonant level at ϵ_d to the closest bath mode. We seek the conditions under which the decay rate approaches the FGR rate predicted from the corresponding continuum model, $\Gamma_{\text{FGR}} = 2\pi |g|^2 / \Delta$.

Again, we are looking for solutions to the equation $z - \epsilon_d - \Sigma_d(z) = 0$, with $\Sigma_d(z) = \sum_n |g|^2 / (z - \epsilon_n)$. As in Eq. (5), we introduce an infinitesimal imaginary part to the bath energies, $\epsilon_n \rightarrow \epsilon_n - i\eta/2$, and in the end take the limit $\eta \rightarrow 0^+$. From the imaginary part of the equation for the poles, we find

$$\chi = - \sum_n \frac{|g|^2 (\eta/2 + \chi)}{(\omega - \epsilon_n)^2 + (\eta/2 + \chi)^2}, \quad (6)$$

where, as before, $z = \omega + i\chi$. Recall that we are looking for poles with a negative imaginary part, $\chi < 0$. Therefore, it must hold that $\eta/2 + \chi > 0$, such that $\Gamma = -2\chi < \eta$. We then find that Γ vanishes upon taking the limit $\eta \rightarrow 0^+$, regardless of the coupling strength g or the mode spacing Δ . The decay rate vanishes due to the manifestly discrete nature of the bath. Taking the limit $\Delta \rightarrow 0$ prior to $\eta \rightarrow 0^+$ would lead to $\Sigma_d(z) = i\pi |g|^2 / \Delta$ at any $\text{Im} z < 0$, and the FGR rate would be recovered. On the contrary, taking the limit $\eta \rightarrow 0^+$ while keeping a small but finite mode spacing Δ retains the discrete structure, such that revival processes occur at times $t = m t_H$, where $m = 1, 2, \dots$, and $t_H = 2\pi/\Delta$ is the Heisenberg time of the bath. These periodic revivals are explicitly present in the following analytic expression for the propagator of the resonant mode in the time domain [3, 48],

$$\begin{aligned} G_d(t) &= e^{-\Gamma_{\text{FGR}} t/2} + \sum_{m=1}^{\infty} e^{-\Gamma_{\text{FGR}}(t - m t_H)/2} e^{i\delta_{\min} m t_H} \\ &\times \Theta(t - m t_H) \sum_{l=0}^{m-1} \binom{m-1}{l} \frac{[-((t - m t_H) \Gamma_{\text{FGR}})]^{m-l}}{(m-l)!}, \end{aligned} \quad (7)$$

where $\Theta(x)$ is the Heaviside function. This implies that the limit $\lim_{t \rightarrow \infty} \mathcal{P}_d(t)$ does not exist.

In order to obtain a finite decay rate, it is necessary to keep finite external broadenings for the bath modes, $\epsilon_n \rightarrow \epsilon_n - i\eta/2$. Formally, η could be obtained by coupling the bath modes a_n to an additional continuous bath, and tracing over the degrees of freedom of the continuous bath. The self-energy becomes

$$\Sigma_d(z) = \frac{\Gamma_{\text{FGR}}}{2} \cot \left(\frac{\pi}{\Delta} (z - \delta_{\min} + i\eta/2) \right), \quad (8)$$

and solving for the equation $z - \epsilon_d - \Sigma_d(z) = 0$ numerically yields the decay rate Γ . The propagator in the time

domain becomes

$$G_d(t) = e^{-\Gamma_{\text{FGR}} t/2} + \sum_{m=1}^{\infty} e^{-\eta m t_{\text{H}}/2} e^{-\Gamma_{\text{FGR}}(t-mt_{\text{H}})/2} e^{i\delta_{\text{min}} m t_{\text{H}}} \times \Theta(t-mt_{\text{H}}) \sum_{l=0}^{m-1} \binom{m-1}{l} \frac{[-((t-mt_{\text{H}})\Gamma_{\text{FGR}})]^{m-l}}{(m-l)!}, \quad (9)$$

such that the m th revival process is attenuated by a factor $e^{-\eta m t_{\text{H}}/2}$. From Eq. (9), it is easy to extract the late-time decay rate in two limiting cases:

$$\Gamma \sim \begin{cases} \eta, & \Gamma_{\text{FGR}} \gg \eta, \Delta, \\ \Gamma_{\text{FGR}}, & \eta \gg \Gamma_{\text{FGR}}, \Delta. \end{cases} \quad (10)$$

Note that the two limits hold for any η/Δ in the first case and any $\Gamma_{\text{FGR}}/\Delta$ in the second case. The intuition behind this result is clear — approaching the thermodynamic limit, $\Delta \rightarrow 0$, the survival probability at large times is dominated by the slower among the decay rate into the bath, Γ_{FGR} , and the escape rate from the bath into the open environment, η . When the mode spacing Δ exceeds both η and Γ_{FGR} , there is no simple asymptotic expression for Γ ; revival processes must be summed coherently, leading to a large time behavior which is sensitive to the position of the resonant level with respect to the equidistant bath modes.

The survival probability, decay rate, and poles of $G_d(z) = 1/(z - \epsilon_d - \Sigma_d(z))$ for the uniform, equidistant bath with $\epsilon_d = \delta_{\text{min}} = 0$ and $\eta/\Delta = 2$ are displayed in Fig. 2. The survival probability clearly illustrates the revival processes occurring at Heisenberg times $t = mt_{\text{H}}$ when the escape rate into the bath, Γ_{FGR} , exceeds the external bath broadening η . In the complex plane, $G_d(z)$ always displays a set of poles at $\text{Im}z = -\eta/2$, separated apart by Δ along the real axis, and there is a pole at $\text{Im}z = -\Gamma_{\text{FGR}}/2$ when $\Gamma_{\text{FGR}} \ll \eta$.

Finally, let us note that for a bath with general coupling coefficients g_n , mode energies ϵ_n , and external broadenings η_n , the decay rate is always bounded by the maximal external broadening of the bath modes. Eq. (6) generalizes to

$$\chi = - \sum_n \frac{g_n^2 (\eta_n/2 + \chi)}{(\omega - \epsilon_n)^2 + (\eta_n/2 + \chi)^2}. \quad (11)$$

Again, since χ must be negative, it must hold that $\eta_n/2 + \chi > 0$ at least for one of the bath modes. In other words, the late-time decay rate is bounded by the maximal bath broadening, $\Gamma = -2\chi < \max_n \{\eta_n\}$.

III. EXPERIMENTAL INTERACTING SYSTEM — JOSEPHSON ARRAY COUPLED TO A COOPER-PAIR BOX

We now depart from the quadratic toy model, and turn to analyze an interacting model of a Josephson array,

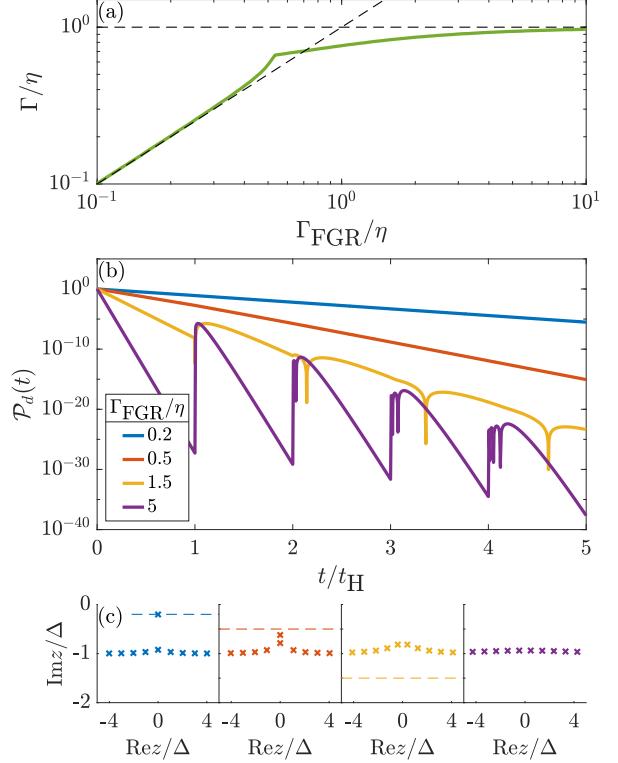


Figure 2. Decay rate for the toy model in Eq. (1) for an equidistant bath, $\epsilon_n = n\Delta$ and $N \rightarrow \infty$, with uniform coupling, $g_n = g$, external broadening $\eta = 2\Delta$, and $\epsilon_d = 0$. (a) Late-time decay rate Γ ($\mathcal{P}_d(t \rightarrow \infty) \sim e^{-\Gamma t}$) as a function of Γ_{FGR}/η . The dashed lines show the asymptotes provided by Eq. (10). (b) Survival probability, $\mathcal{P}_d(t) = |G_d(t)|^2$, given by Eq. (9). (c) The poles of the propagator $G_d(z)$ in the complex plane. The dashed lines are at $\text{Im}z = -\Gamma_{\text{FGR}}/2$.

implementing a nearly quadratic transmission line, terminated by a nonlinear impurity. The Josephson array is diagonalized by photonic modes, which are coupled to one another via wave-mixing terms provided by the impurity, such that each single-photon state is coupled to many multi-photon states. For any given n , we refer to the set of n -photon states as a bath.

As before, in order to discuss the long-time decay rate, we must introduce some broadening of the modes by an external environment. This broadening is inherently present in any experimental system, due to loss mechanism in the array that are unrelated to the wave-mixing terms provided by the impurity. The origin of these mechanisms could be both internal, such as quasiparticle poisoning [49] or two-level-system dielectric loss [50], as well as external, due to the capacitive coupling of the array to the antenna used for spectroscopy. We incorporate these loss mechanisms into the calculation by assigning each mode some initial broadening; note that this broadening may be directly probed in an experiment by dis-

connecting the impurity and measuring the internal and external quality factors of the system eigenmodes [44].

In this Section, we derive an expression for the propagator of the single-photon modes. We identify the contributions of the different baths, and, following our discussion in Section II, analyze the decay rate induced by each bath. Applying a self-consistent approach, we show how the convergence of the decay rate induced by some bath to its FGR rate is accelerated by the presence of other baths, due to cascade decay processes into lower-frequency modes, depicted in Fig. 1.

For concreteness, in the following, we consider a Cooper-pair box impurity, implementing a discrete analog of the boundary sine-Gordon model, although our formalism applies to any type of impurity, and also to wave-mixing terms originating from weak bulk nonlinearities.

A. Hamiltonian and eigenmodes

Consider the Hamiltonian of a Josephson array coupled to a Cooper-pair box (setting $\hbar = e = 1$ henceforth), sketched in Fig. 1,

$$\mathcal{H} = \sum_{i,j=0}^N 2 [C^{-1}]_{i,j} Q_i Q_j - \sum_{i=1}^N E_J^{\text{line}} \cos(\phi_i - \phi_{i-1}) - E_J \cos(\phi_0), \quad (12)$$

where ϕ_i and Q_i are the superconducting phase and charge of the i th superconducting grain, respectively. The matrix C^{-1} is the inverse of the capacitance matrix C , which is a tridiagonal matrix with $C_{0,0} = C_0 + C^{\text{line}}$, $C_{i,i-1} = C_{i-1,i} = -C^{\text{line}}$, $C_{i,i} = C_g + 2C^{\text{line}}$ for $1 \leq i \leq N-1$, and $C_{N,N} = C_g + C^{\text{line}}$. The Josephson energies E_J^{line} and intergrain capacitances C^{line} are chosen such that $E_J^{\text{line}} \gg E_C^{\text{line}}$, where $E_C^{\text{line}} = 1/(2C^{\text{line}})$, so that anharmonic effects and phase slips are suppressed in the line, and the Josephson terms of the array may be replaced by $(\phi_i - \phi_{i-1})^2 / (8L^{\text{line}})$, with $L^{\text{line}} = 1/(4E_J^{\text{line}})$. Treating the boundary cosine term as a perturbation, the quadratic part of the Hamiltonian is diagonalized by plane waves, $\phi_i = \sum_k \phi_k \sin(ki + \delta_k)$ (where we set the grain spacing to unity), with the oscillatory behavior $\ddot{\phi}_k = -\omega_k^2 \phi_k$. The dispersion relation reads $\omega_k \approx vk / \sqrt{1 + (vk/\omega_p)^2}$, with $v = 1/\sqrt{L^{\text{line}}C_g}$ and $\omega_p = 1/\sqrt{L^{\text{line}}C^{\text{line}}}$, and, assuming $v \gg \omega_p$, the phase shift is given by $\tan \delta_k \approx -\Gamma_0 \sqrt{1 - (\omega_k/\omega_p)^2} / \omega_k$. Here $\Gamma_0 = 1/(ZC_0)$ is the inverse RC time of the array and the Cooper-pair box, and $Z = \sqrt{L^{\text{line}}/C_g}$ is the impedance of the line. In the following, we denote the normalized impedance by $z = Z/R_Q$, where $R_Q = h/(4e^2) = \pi/2$ is the resistance quantum. Open boundary conditions at $i = N$ lead to the quantization condition $kN + \delta_k = \pi l$,

where $l = 0, 1, \dots, N-1$, giving rise to the k -dependent mode spacing, $\Delta_k = \Delta \left(1 - (\omega_k/\omega_p)^2\right)^{3/2}$, with $\Delta = \pi v/N$.

B. Self-energy and multi-photon baths

Introducing creation and annihilation operators, $\phi_k = \sqrt{2z\Delta \left(1 - (\omega_k/\omega_p)^2\right)} / \omega_k (a_k + a_k^\dagger)$, leads to $\mathcal{H} = \mathcal{H}_0 + \mathcal{H}_I$, where the free Hamiltonian is $\mathcal{H}_0 = \sum_k \omega_k a_k^\dagger a_k$, and the interaction term reads $\mathcal{H}_I = -E_J \cos\left(\sum_k f_k (a_k + a_k^\dagger)\right)$, with

$$f_k^2 = \frac{2z\Delta}{\omega_k} \frac{\left(1 - (\omega_k/\omega_p)^2\right)^2}{1 + \left((\omega_p/\Gamma_0)^2 - 1\right) (\omega_k/\omega_p)^2}. \quad (13)$$

Throughout this work, we assume $E_J \ll E_C$ with $E_C = 1/(2C_0)$, such that \mathcal{H}_I can be treated as a perturbation. Note that \mathcal{H}_I is relevant in an RG sense for $z < 1$ [51], and there is an emergent RG scale, $E_J^* \sim (E_J/\omega_c^z)^{1/(1-z)}$, where $\omega_c \sim \min\{\omega_p, \Gamma_0\}$ is a UV cutoff, such that perturbation theory applies only at $\omega_k \gg E_J^*$. \mathcal{H}_I is irrelevant for $z > 1$, such that $E_J^* = 0$, and perturbation theory applies at all frequencies. In the following, we address the perturbative regime. To second order in E_J , the time-ordered propagator of the k th mode, $G_k(t) = -i \langle \mathcal{T} \phi_k(t) \phi_k(0) \rangle$, is given in the frequency domain by

$$G_k(\omega) = \frac{4z\Delta \left(1 - (\omega_k/\omega_p)^2\right)}{\omega^2 - [\omega_k - (\Sigma_k(\omega) - \text{Re}\Sigma_k(\omega = 0))]^2}, \quad (14)$$

with the self-energy (at $T = 0$) [31]

$$\Sigma_k(\omega) = 2iE_J^2 f_k^2 \int_{-\infty}^{\infty} dt e^{i\omega t} \langle \mathcal{T} \sin(\phi_0(t)) \sin(\phi_0(0)) \rangle_{\mathcal{H}_0}, \quad (15)$$

where the expectation value is calculated with respect to \mathcal{H}_0 . Using the eigenmode expansion of ϕ_0 and the Campbell-Baker-Hausdorff formula, we find:

$$\Sigma_k(\omega) = 2iE_J^2 f_k^2 e^{-\sum_{k'} f_{k'}^2} \times \int_{-\infty}^{\infty} dt e^{i\omega t} \sinh \left\{ \sum_{k'} i f_{k'}^2 \tilde{G}_{k'}^{(0)}(t) \right\}, \quad (16)$$

where $\tilde{G}_k^{(0)} = -i \langle \mathcal{T} (a_k(t) + a_k^\dagger(t)) (a_k(0) + a_k^\dagger(0)) \rangle_{\mathcal{H}_0}$ is the free propagator of the k th mode (without the prefactor appearing in ϕ_k), given by

$$\tilde{G}_k^{(0)}(\omega) = \frac{2\omega_k}{\omega^2 - (\omega_k - i\Gamma^b/2)^2}. \quad (17)$$

Note that we introduce some finite broadening, Γ^b , to each of the free propagators. Similarly to Section II, Γ^b could be formally obtained by coupling the free modes to a larger environment and tracing over the degrees of freedom of the environment. This broadening is due internal and external dissipation processes in the array which are unrelated to the impurity at $i = 0$, is always present in an experimental environment, and can be assumed to be the smallest energy scale in the system, several orders of magnitude below the mode spacing Δ [44].

Expanding the hyperbolic sine in Eq. (16), we find $\Sigma_k(\omega) = \sum_{n=0}^{\infty} \Sigma_{k;2n+1}(\omega)$, with

$$\Sigma_{k;2n+1}^b(\omega) = \frac{2iE_J^2 f_k^2 e^{-\sum_{k'} f_{k'}^2}}{(2n+1)!} \times \int_{-\infty}^{\infty} dt e^{i\omega t} \left[\sum_{k'} i f_{k'}^2 \tilde{G}_{k'}^{(0)}(t) \right]^{2n+1}. \quad (18)$$

$\Sigma_{k;2n+1}^b(\omega)$ is the contribution of the bath of $2n+1$ photon modes to the self-energy $\Sigma_k^b(\omega)$. The superscript b indicates that the self-energy is evaluated using the bare propagators, $\tilde{G}_{k'}^{(0)}(t)$, and stands to distinguish it from the self-consistent self-energy, to be discussed below. To understand the structure of $\Sigma_{k;2n+1}^b(\omega)$, it is useful to expand the product and express the result in terms of the frequency-domain bare propagators:

$$\Sigma_{k;2n+1}^b(\omega) = \frac{2iE_J^2 f_k^2 e^{-\sum_{k'} f_{k'}^2}}{(2n+1)!} \sum_{k_1, \dots, k_{2n+1}} \prod_{i=1}^{2n+1} f_{k_i}^2 \times \frac{1}{(2\pi)^{2n}} i\tilde{G}_{k_1}^{(0)}(\omega) * \dots * i\tilde{G}_{k_{2n+1}}^{(0)}(\omega), \quad (19)$$

where $*$ denotes convolution. Eq. (19) shows that the self-energy decomposes into a sum over baths of $2n+1$ photons, where each many-body state of $2n+1$ photons contributes a Lorentzian centered around $\sum_{i=1}^{2n+1} \omega_{k_i}$ with a width of $(2n+1)\Gamma^b$. The weight of each Lorentzian in $\Sigma_{k;2n+1}^b(\omega)$ is determined by a product of factors $f_{k_i}^2$ of the modes k_i that form the $2n+1$ -photons mode; since $f_k^2 \sim 1/\omega_k$, the leading contribution originates from many-body states involving many low-frequency modes.

C. Decay rate in the thermodynamic limit

Consider the thermodynamic limit, $N \rightarrow \infty$, such that $\Delta \rightarrow 0$ and the modes of \mathcal{H}_0 form a continuum. In that case, following the discussion in Section II, the decay rate of a mode k induced by the bath of $2n+1$ photons is given by the imaginary part of the respective self-energy evaluated at $\omega = \omega_k$, $\Gamma_{k;2n+1}^{\text{FGR}} = 2\text{Im}\Sigma_{k;2n+1}(\omega_k)$. Using the unbroadened free propagators, $i\tilde{G}_k^{(0)}(t) = e^{-i\omega_k|t|}$, we

have

$$\Gamma_{k;2n+1}^{\text{FGR}} = \frac{2E_J^2 f_k^2 e^{-\sum_{k'} f_{k'}^2}}{(2n+1)!} \times \int_{-\infty}^{\infty} dt e^{i\omega_k t} \left[\sum_{k'} f_{k'}^2 e^{-i\omega_{k'} t} \right]^{2n+1}. \quad (20)$$

To illustrate the structure of $\Gamma_{k;2n+1}^{\text{FGR}}$, it is useful to expand the brackets inside the integral and carry out the integration over time. We arrive at

$$\Gamma_{k;2n+1}^{\text{FGR}} = \frac{2E_J^2 f_k^2 e^{-\sum_{k'} f_{k'}^2}}{(2n+1)!} \sum_{k_1, \dots, k_{2n+1}} \prod_{i=1}^{2n+1} f_{k_i}^2 \times 2\pi\delta(\omega_k - \omega_{k_1} - \dots - \omega_{k_{2n+1}}), \quad (21)$$

which shows that the decay rate induced by $1 \rightarrow 2n+1$ decay processes is given by a sum over all $2n+1$ -photon states with energy equal to ω_k . In practice, it is more convenient to evaluate $\Gamma_{k;2n+1}^{\text{FGR}}$ using Eq. (20); however, Eq. (20) involves a sum over the discrete modes, which we would like to convert into an integral over the continuum of modes in the thermodynamic limit, $\sum_{k'} \rightarrow \int d\omega'/\Delta(\omega')$. Since the integral is IR-divergent, $f_k^2 \sim 1/\omega_k$, one must keep a finite IR cutoff, $\Delta/2$ (the lowest frequency mode), that gives rise to a time-dependent factor, denoted here by $\gamma_{1/2}(t)$, which is formally given by the Euler-Maclaurin summation formula, and whose origin is similar to that of the Euler-Mascheroni constant, $\gamma = \int_1^{\infty} dx (1/[x] - 1/x) \approx 0.5772$ (where $[x]$ is the integer part of x):

$$\sum_{k'} f_{k'}^2 e^{-i\omega_{k'} t} \approx \int_{\Delta/2}^{\omega_p} d\omega' \frac{f^2(\omega') e^{-i\omega' t}}{\Delta(\omega')} + 2z\gamma_{1/2}(t). \quad (22)$$

Note that $f_k^2 \sim \Delta$, such that f_k^2/Δ is finite in the limit $\Delta \rightarrow 0$. The factor $\gamma_{1/2}(t)$ varies slowly on a scale of $1/\Delta$, so that in the thermodynamic limit, $\Delta \rightarrow 0$, it may be replaced by its value at $t = 0$:

$$2z\gamma_{1/2} = \sum_{k'} f_{k'}^2 - \int_{\Delta/2}^{\omega_p} d\omega' \frac{f^2(\omega')}{\Delta(\omega')}. \quad (23)$$

The factor $\gamma_{1/2}$ depends weakly on $\Delta, \Gamma_0, \omega_p$, and, in the limit $\Delta \ll \Gamma_0, \omega_p$, we may approximate

$$\gamma_{1/2} \approx \int_0^{\infty} dx \left(\frac{1}{[x] + 1/2} - \frac{1}{x + 1/2} \right) \approx 1.27. \quad (24)$$

Plugging everything into $\Gamma_{k;2n+1}^{\text{FGR}}$, we find:

$$\Gamma_{k;2n+1}^{\text{FGR}} = \frac{2E_J^2 f_k^2}{(2n+1)!} e^{-\int_{\Delta/2}^{\omega_p} d\omega' f^2(\omega')/\Delta(\omega')} e^{-2z\gamma_{1/2}} \times \int_{-\infty}^{\infty} dt e^{i\omega t} \left[\int_{\Delta/2}^{\omega_p} \frac{d\omega'}{\Delta(\omega')} f^2(\omega') e^{-i\omega' t} + 2z\gamma_{1/2} \right]^{2n+1}. \quad (25)$$

Eq. (25) yields the FGR result for the decay rate induced by the $2n+1$ -photon bath, and may be evaluated numerically. To gain analytical insight, it is useful to approximate $f^2(\omega')/\Delta(\omega') \approx 2ze^{-\omega'/\omega_c}/\omega'$, where ω_c is the cutoff frequency, given approximately by $\omega_c \sim \min\{\omega_p, \Gamma_0\}$, and let $\omega_p \rightarrow \infty$ for the upper integration limit of $\int d\omega'$. This leads to

$$\Gamma_{k;2n+1}^{\text{FGR}} = \frac{2E_J^2 f_k^2}{(2n+1)!} e^{-2z} \int_{\Delta/2}^{\infty} d\omega' e^{-\omega'/\omega_c} e^{-2z\gamma_{1/2}} \times \int_{-\infty}^{\infty} dt e^{i\omega_k t} \left[2z \int_{\Delta/2}^{\infty} \frac{d\omega'}{\omega'} e^{-\omega'/\omega_c} e^{-i\omega' t} + 2z\gamma_{1/2} \right]^{2n+1}, \quad (26)$$

which is evaluated in Appendix A. The leading contribution reads $\Gamma_{k;2n+1}^{\text{FGR}}/\Delta \sim \Delta^{2z} \times 1/\omega_k^2 \times \log^{2n}(\omega_k/\Delta)$; therefore, taking the thermodynamic limit, the decay rate of each bath vanishes as power law in the system size, N^{-2z} , with some logarithmic corrections. However, the total decay rate $\Gamma_k^{\text{FGR}}/\Delta = \sum_{n=1}^{\infty} \Gamma_{k;2n+1}^{\text{FGR}}/\Delta$ remains finite, and is given by a Luttinger-liquid power law, $\Gamma_k^{\text{FGR}}/\Delta \sim \omega_k^{2z-2}$.

The decay rates of the baths in the thermodynamic limit are shown in Fig. 3. The sum of rates agrees quantitatively with the total decay rate,

$$\Gamma_k^{\text{FGR}}/\Delta = \frac{2\pi z}{\Gamma(2z)} \frac{E_J^2 \omega_k^{2z-2}}{\omega_c^{2z}} e^{-2\omega_k/\omega_c}, \quad (27)$$

which was derived in Ref. [31]. Note that for any n , the decay rate of the $2n+1$ -photon bath $\Gamma_{k;2n+1}^{\text{FGR}}$ approaches 0 at large enough ω_k/Δ ; this decrease is countered by the emergence of new decay channels with higher n as ω_k increases. It is interesting to note that at the Schmid-Bulgadaev transition, $z = 1$, the decrease in the rate of the existing decay channels is exactly balanced by the emergence of the new channels to produce a constant total decay rate at frequencies $\Delta \ll \omega_k \ll \Gamma_0$.

D. Decay rate at finite N

1. Approaching the thermodynamic limit

Having obtained the FGR rates in the thermodynamic limit, we are now interested in the decay rates for a finite array size N . First, let us argue that, when N is large enough (though finite) while all other parameters are held fixed, Eq. (25) evaluated at finite Δ indeed corresponds to the decay rates of the baths. This follows from the discussion of the toy model in Section II, where it was shown that, for external broadening η that is significantly larger than both the FGR rate and the mode spacing (see Eq. (10)), the decay rate is equal to the FGR rate. Considering the $2n+1$ -photon bath, its structure is revealed by Eq. (19); it is composed of many Lorentzians whose width is $(2n+1)\Gamma^b$, in analogy to the external broadening η of the modes in the

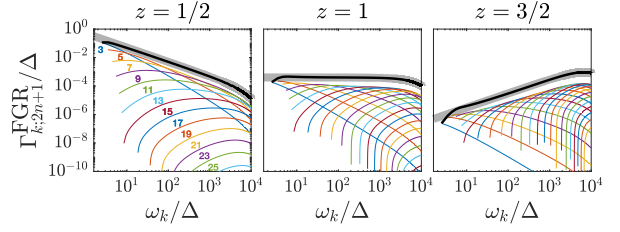


Figure 3. Decay rates in the thermodynamic limit. The colored lines depict the decay rates of the baths of $2n+1$ photons; the decay rate of the $2n+1$ photons bath is plotted only for frequencies satisfying $\omega_k > (2n+1)\Delta/2$. The bath indices $N_{\text{out}} = 2n+1$ are written explicitly next to the lines in the $z = 1/2$ panel, and the order of the lines is the same in the $z = 1$ and $z = 3/2$ panels — the blue line that starts on the top left shows the 3-photon rate, the succeeding orange line shows the 5-photon rate, and so on. The black line is the sum of all rates, $\Gamma_k^{\text{FGR}} = \sum_{n=1}^{\infty} \Gamma_{k;2n+1}^{\text{FGR}}$, and the thick grey line is the expected result from Ref. [31], given by Eq. (27). The parameters used in this figure are $\omega_p \rightarrow \infty$, $\Gamma_0/\Delta = 10^4$, and $E_J/\Delta = 20, 50, 200$ for $z = 1/2, 1, 3/2$, respectively.

toy model. The mode spacing of $2n+1$ -photon states is given by $\Delta_{2n+1}(\omega) = (2n)! \times \Delta^{2n+1}/\omega^{2n}$, and the FGR rate scales as $\Gamma_{k;2n+1}^{\text{FGR}} \sim \Delta^{2z+1}/\omega_k^2$ up to logarithmic corrections, where $\Delta \sim 1/N$. We thus find that for fixed Γ^b and any ω_k , there is a crossover scale for the array size, N_{2n+1}^{FGR} , defined by the conditions of the latter case of Eq. (10), namely, $\Gamma_{k;2n+1}^{\text{FGR}} \ll (2n+1)\Gamma^b$ and $\Delta_{2n+1}(\omega_k) \ll (2n+1)\Gamma^b$. Each of these inequalities defines a crossover scale, with N_{2n+1}^{FGR} set by the larger of them; then, for $N \gg N_{2n+1}^{\text{FGR}}$, we have $\Gamma_{k;2n+1}^{\text{in}} \rightarrow \Gamma_{k;2n+1}^{\text{FGR}}$. N_{2n+1}^{FGR} scales with frequency as $N_{2n+1}^{\text{FGR}} \sim \omega_k^{-\nu}$, with $\nu = \max\{2n/(2n+1), 2/(2z+1)\}$, such that the FGR regime is reached faster (i.e. smaller N) at larger frequencies, which can decay into a larger set of combinations of low-frequency photons. Note that N_{2n+1}^{FGR} depends on the order of the bath n , such that different baths enter the FGR regimes at different array sizes. This would be important in the following to understand the cross-bath broadening.

Let us stress again that the order of limits is crucial; taking $\Gamma^b \rightarrow 0$ and only then letting $N \rightarrow \infty$ would lead to a vanishing decay rate. In the following, we show the convergence to the FGR rate for a given bath is accelerated by the presence of the other baths, using a self-consistent calculation.

2. Self-consistent approach

As discussed in Section II, the crossover into the FGR regime is determined by the ratio of the FGR decay rate and the external broadening of the bath modes. It is evident from Eq. (19) that the bath of some mode k is formed by many-body states involving the other modes k' , which are themselves broadened by nonlinear scattering off the

impurity. In order to incorporate these cascades into the self-energy of the mode k , we replace the free propagators $\tilde{G}_k^{(0)}$ in Eq. (18) with the dressed propagators \tilde{G}_k^{dr} :

$$\Sigma_{k;2n+1}^{\text{dr}}(\omega) = \frac{2iE_J^2 f_k^2 e^{-\sum_{k'} f_{k'}^2}}{(2n+1)!} \times \int_{-\infty}^{\infty} dt e^{i\omega t} \left[\sum_{k'} i f_{k'}^2 \tilde{G}_{k'}^{\text{dr}}(t) \right]^{2n+1}. \quad (28)$$

The dressed propagators \tilde{G}_k^{dr} are calculated with the dressed self-energies $\Sigma_{k;2n+1}^{\text{dr}}$,

$$\tilde{G}_k^{\text{dr}}(\omega) = \frac{2\omega_k}{\omega^2 - [\omega_k - (\Sigma_k^{\text{dr}}(\omega) - \text{Re}\Sigma_k^{\text{dr}}(\omega=0)) - i\Gamma^b/2]^2}, \quad (29)$$

where $\Sigma_k^{\text{dr}} = \sum_n \Sigma_{k;2n+1}^{\text{dr}}$. Eq. (28) thus defines a set of $N+1$ (one for each mode k) coupled integral equations, which are very difficult to solve. This formidable task may be greatly simplified by taking advantage of the structure of the self-energy in Eq. (19). As mentioned above, each state of $2n+1$ photons contributes a Lorentzian centered around $\sum_{i=1}^{2n+1} \omega_{k_i}$. In the evaluation of the propagator G_k of some mode k , we are only interested in the self-energy Σ_k at frequencies $\omega \sim \omega_k$; the contribution of states with $|\sum_{i=1}^{2n+1} \omega_{k_i} - \omega_k| \gtrsim \Delta$ is negligible. In particular, states of $2n+1$ photons involving modes $k' \geq k$ can be discarded in the evaluation of Σ_k — namely,

$$\Sigma_{k;2n+1}^{\text{dr}}(\omega) \approx \frac{2iE_J^2 f_k^2 e^{-\sum_{k'} f_{k'}^2}}{(2n+1)!} \times \int_{-\infty}^{\infty} dt e^{i\omega t} \left[\sum_{k' < k} i f_{k'}^2 \tilde{G}_{k'}^{\text{dr}}(t) \right]^{2n+1}. \quad (30)$$

In other words, the self-energy Σ_k^{dr} and propagator G_k^{dr} depend only on propagators at lower modes, $k' < k$, and the self-consistent equations may be solved iteratively in a single run over the modes.

Let us note that the modes $k' \geq k$ could affect the elastic mode shift $\Delta\omega_k \sim \text{Re}\Sigma_k(\omega_k)$ induced by the interaction Hamiltonian \mathcal{H}_I . We assume that the contribution of the terms corresponding to the modes $k' \geq k$ is negligible compared to the rest of the terms; we also introduce some disorder in our numerical calculations (see below), which masks the effect of the elastic phase shift.

The self-consistent approach accounts for the broadening of the propagators induced by all of the baths. In order to highlight the interplay between the different baths, we also apply a partial self-consistent approach, in which we evaluate the self-energy

$$\Sigma_{k;2n+1}^{\text{p}}(\omega) = \frac{2iE_J^2 f_k^2 e^{-\sum_{k'} f_{k'}^2}}{(2n+1)!} \times \int_{-\infty}^{\infty} dt e^{i\omega t} \left[\sum_{k' < k} i f_{k'}^2 \tilde{G}_{k';2n+1}^{\text{p}}(t) \right]^{2n+1}, \quad (31)$$

where $\tilde{G}_{k';2n+1}^{\text{p}}$ is the propagator broadened only by the bath of $2n+1$ photons:

$$\tilde{G}_{k';2n+1}^{\text{p}}(\omega) = 2\omega_{k'} / \left\{ \omega^2 - \left[\omega_{k'} - i\Gamma^b/2 - \left(\Sigma_{k';2n+1}^{\text{p}}(\omega) - \text{Re}\Sigma_{k';2n+1}^{\text{p}}(\omega=0) \right) \right]^2 \right\}. \quad (32)$$

This partial approach incorporates the broadening that each bath imposes on itself, but ignores inter-bath broadening.

3. Numerical evaluation of the decay rates

In the following, we evaluate the decay rate induced by a Cooper-pair box impurity at finite array size N . We initialize all propagators with some external broadening Γ^b , and evaluate the self-energy using Eqs. (18), (30), or (31). We plug the self-energies into the propagator,

$$G_k(\omega) = \frac{4z\Delta \left(1 - (\omega_k/\omega_p)^2 \right)}{\omega^2 - [\omega_k - (\Sigma_k(\omega) - \text{Re}\Sigma_k(\omega=0)) - i\Gamma^b/2]^2}. \quad (33)$$

calculate the inverse Fourier transform to get $G_k(t)$, and extract the decay rate Γ_k^{in} from the late-time dynamics by fitting $G_k(t \rightarrow \infty)$ to a decaying exponential $e^{-\Gamma_k^{\text{in}} t}$.

We use experimentally-relevant parameters, specified in the caption of Fig. 4. Importantly, we use the normalized impedance $z = 1/2$, where the FGR decay rates decrease rapidly with the order of the bath, as discussed in Section III C and illustrated in Fig. 3. We discard the contributions of baths with $2n+1 \geq 11$, which are negligible. Note that it is crucial to keep a finite plasma frequency ω_p in our calculations; in the limit $\omega_p \rightarrow \infty$ and $v \rightarrow \infty$, the dispersion relation is nearly linear, $\omega_k \approx vk$, leading to a massive degeneracy of the many-body modes. In addition to keeping ω_p finite, we introduce some disorder that spreads out the many-body modes. Some details regarding the added disorder, as well as a discussion of RG considerations at low-frequency modes, are given in Appendix B.

4. Results and discussion

The decay rates as a function of ω_k at fixed N , as well as a function of N at fixed ω_k , are shown in Fig. 4. The decay rates induced by each of the baths, $\Gamma_{k;2n+1}^{\text{in}}$, agree with the general result of Eq. (10) derived for the toy model in the respective limits, and, in particular, $\Gamma_{k;2n+1}^{\text{in}} \rightarrow \Gamma_{k;2n+1}^{\text{FGR}}$ at large enough ω_k/Δ or N . At small ω_k/Δ or N , the decay rate of the $2n+1$ -photon bath is given by $(2n+1)\Gamma^b$. Note that, for the 7-photon bath, we find that $\Gamma_{k;7}^{\text{in}} \sim \Gamma_{k;7}^{\text{FGR}}$ at most frequencies, since the bare broadening of the 7-photon modes is larger than the

FGR rate, $\Gamma_{k;7}^{\text{FGR}} < 7\Gamma^{\text{b}}$, at most frequencies. A similar result is obtained for the 9-photon bath, not shown in Fig. 4. The oscillations of the decay rates with frequency at small ω_k/Δ are due to the convexity of the dispersion relation, $\omega_k \approx vk/\sqrt{1 + (vk/\omega_p)^2}$, which shifts the energies of the many-body states with respect to those of the single-photon states, as illustrated in Fig. 1. The 3- and 5-photon baths, on the other hand, display a crossover between the two regimes.

The effect of the cascade decay processes is clearly illustrated by the crossover region between small and large ω_k/Δ or N . As expected, the dressed propagator yields a larger decay rate than that of the bare propagator. The dressing accelerates the convergence of the decay rates to their FGR values with either frequency or array size, and, importantly, enhances the maximally-allowed decay rate induced by each bath. In Section II, we showed that the decay rate induced by a bath is necessarily bounded by the largest broadening of the bath modes, such that, when the bare propagator G_k^{b} is considered (that is, excluding cascade processes), it must hold that $\Gamma_{k;2n+1}^{\text{in}} < (2n+1)\Gamma^{\text{b}}$. However, the dressing broadens the bath states; therefore, the decay rate of the $2n+1$ -photon bath extracted from the dressed propagator may in fact exceed $(2n+1)\Gamma^{\text{b}}$.

While the accelerated crossover to the FGR regime and the enhancement of the maximally-allowed decay rates occur for both partial (G_k^{p}) and full (G_k^{dr}) dressing, these effects are particularly prominent in the latter case, as demonstrated by Fig. 4. That is, the decay rate into the n -photon bath is enhanced by the presence of $m \neq n$ -photon baths. This is due to the different convergence rates of the baths to their FGR regimes; as discussed above, each bath is characterized by a crossover scale for the array size N_{2n+1}^{FGR} , which depends on the bath order $2n+1$. For a Cooper-pair box impurity with $z = 1/2$, we find that baths formed by many-photon states enter the FGR regime and induce a large decay rate faster than baths of few-photon states. This is most evident for the 3-photon bath — there is a range of modes that are not in the FGR regime of the 3-photon bath (i.e. $\Gamma_{k;3}^{\text{in}} < \Gamma_{k;3}^{\text{FGR}}$), which are broadened by the 5-, 7-, and 9-photon baths, such that the single-photon modes in this range are broadened beyond Γ^{b} . Therefore, when a mode k in this range decays into 3-photon states involving another mode in this range ($\omega_k \rightarrow \omega_k + \omega_{k''} + \omega_{k'''}$, where $k' \lesssim k$ and k'', k''' are low frequency modes), the total broadening of the outgoing 3-photon state exceeds $3\Gamma^{\text{b}}$, and therefore $\Gamma_{k;3}^{\text{in}} > 3\Gamma^{\text{b}}$ is allowed. This effect accelerates the convergence of $\Gamma_{k;3}^{\text{in}}$ to its FGR value; the condition for the FGR to apply is then $\Gamma_{k;3}^{\text{FGR}} < \bar{\eta}_3$, where $\bar{\eta}_3$ is the average width of the 3-photon states, which takes into account the broadening induced by the cascade decay processes.

Fig. 4 also shows the self-energies and the propagator of one of the modes at some given array size N . The sharp features of the propagator $G_k(\omega)$ are due to

level repulsion between the single-photon mode at ω_k and the many-body states at comparable frequencies, which appear in the self-energies. The fully-dressed propagator G_k^{dr} and self-energies $\Sigma_{k;2n+1}^{\text{dr}}$ are generally smoother than their bare and partially-dressed counterparts (as most clearly illustrated by the difference between $\Sigma_{k;3}^{\text{dr}}$ and $\Sigma_{k;3}^{\text{b}}, \Sigma_{k;3}^{\text{p}}$), since the Lorentzians in the dressed self-energies (see Eq. (19)) are smeared out by the broadening of the single-photon states comprising the multi-photon states. Fig. 5 further shows the spectral function of the fully-dressed propagator for two different array sizes at some given frequency — as expected, level repulsion is a lot more prominent for shorter array size.

The level repulsion in $G_k(\omega)$ may be observed in a spectroscopy experiment, and was reported in Ref. [36] for a fluxonium impurity, where the self-energies of the single-photon modes are dominated by the contributions of the 2- and 3-photon baths. Our calculation provides a prediction for the spectral function probed in such an experiment, and could be applied to any nonlinearity (located either at the boundary or in the bulk) with any number of multi-photon baths. Importantly, let us note that the absence of anticrossings in the spectroscopy measurement does not necessarily imply that the single-photon decoheres with the FGR rate. Its coherence time could be longer than its apparent lifetime extracted from the width of the Lorentzian, if the condition $\bar{\eta} \gg \Gamma_k^{\text{FGR}}$ is not met, where $\bar{\eta}$ is the average width of the multi-photon levels that couple to the single-photon state. Indeed, if $\Gamma_k^{\text{FGR}} \gtrsim \bar{\eta}$ and $\Delta_n \ll \bar{\eta}$ for the multi-photon mode spacings Δ_n , the propagator $G_k(\omega)$ would form a smooth Lorentzian with a width Γ_k^{FGR} , yet revival processes at large times would still occur, and the long-time decoherence rate Γ would be smaller than Γ_k^{FGR} .

IV. CONCLUSIONS

In this work, we showed how the FGR emerges in the decay of a single-photon when the system approaches the thermodynamic limit. Keeping a finite bare decoherence rate, necessary to obtain an exponential decay of the single-photon states in the long-time limit for any finite system size, we derived the conditions for the rates induced by the multi-photon baths to reach the values predicted by the FGR. We calculated the self-energies of the single-photon propagators in a self-consistent manner, and showed that the crossover of the n -photon bath into the FGR regime is accelerated by the presence of the other $m \neq n$ -photon baths, due to cascade decay processes into low-frequency modes.

This work provides a framework to analyze the experiment in Ref. [36], and allows one to reproduce the measured single-photon spectroscopy picture. The level repulsion between single- and multi-photon states reported in Ref. [36] is clearly visible in Fig. 4, and our calculations should apply to any bath with any number of photons, and any type of weak bulk or boundary nonlinearity. As

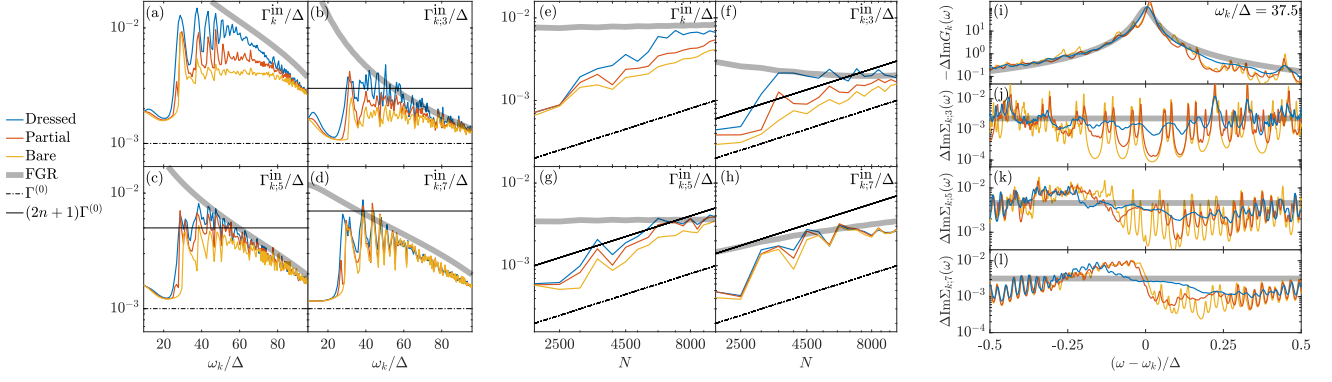


Figure 4. (a)-(d) Decay rates as a function of frequency extracted from the propagators in the time-domain, evaluated from Eq. (33), with the self-energy given by Eqs. (30) (dressed), (31) (partial), and (18) (bare), for $N = 10^4$. (a) Decay rate induced by the total self-energy Σ_k . (b)-(d) Decay rates induced by the baths of 3-, 5-, and 7-photon states. All decay rates were averaged over 50 realizations of disorder. (e)-(h) Decay rates as a function of N for $\omega_k = 0.6 \times \omega_p$. (i)-(l) Spectral function and imaginary part of the self-energies $\Sigma_{k;2n+1}$ of the mode at $\omega_k/\Delta = 37.5$ with $N = 10^4$, for a single realization of disorder. In all plots, the thick grey line shows the results predicted by the FGR. The experimentally-relevant parameters used for this figure are $E_J = 1$ GHz, $E_C = 20$ GHz, $z = 1/2$, $\omega_p = 20$ GHz, and $v = 3.33$ THz (in units of the intergrain spacing a), such that, at $N = 10^4$, $\Delta = 0.167$ GHz, and $\Gamma^b/\Delta = 10^{-3}$.

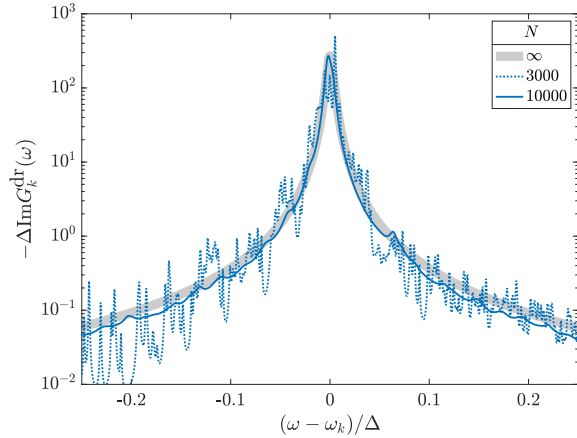


Figure 5. Spectral function extracted from the fully-dressed propagator of the mode at $\omega_k = 0.6 \times \omega_p$ for two values of the array size N , each for a single realization of disorder. The thick grey line shows the spectral function for a semi-infinite array. The parameters used are the same as in Fig. 4.

discussed above, the absence of level repulsions does not necessarily imply that the single-photon decoheres with the FGR rate, since the decoherence rate could still be limited by the bare decoherence rate of the array modes, which is unrelated to the bulk or boundary nonlinearity. In the context of quantum information processing, this effect could be leveraged to engineer a system of a finite multimode resonator superstrongly coupled to a qubit to harvest such revival processes and prolong the lifetime of the single-photon and qubit states.

As mentioned above, the emergence of the FGR is closely related to questions about thermalization in large

many-body systems, Fock-space delocalization, and the onset of chaos [12, 20, 52], which have also been discussed recently in the context of circuit quantum electrodynamics [53]. Let us note that in this work we considered a Cooper-pair box impurity, which, upon taking the scaling limit $E_J, \omega_c \rightarrow \infty$ (where $\omega_c \sim \min\{\Gamma_0, \omega_p\}$) with $E_J^* = (E_J/\omega_c^z)^{1/(1-z)}$ fixed (for $z < 1$), leads to the boundary sine-Gordon model, which is integrable [54]. Our results imply that the FGR should still emerge in the boundary sine-Gordon model, despite of its integrability, with the exact inelastic decay rates in the thermodynamic limit calculated in Ref. [32]. The emergence of inelastic decay in integrable systems raises an analogous question in the context of thermalization. Ref. [53] demonstrated that a closed system with a generic three-wave mixing term, initialized in some excited state, relaxes to a Bose-Einstein distribution of photons. While it is well-known that integrable systems thermalize into generalized Gibbs ensembles [55], could the cosine nonlinearity of the (closed) boundary sine-Gordon model still give rise to a standard Bose-Einstein distribution of the photons (which are not the eigenstates of the Hamiltonian)? And if so, how is the convergence rate to this distribution related to the FGR? We leave these questions as a future perspective.

Acknowledgements

We would like to thank Ehud Altman, Boris Altshuler, Anushya Chandran, Roman Kuzmin, and Maxim Vavilov for fruitful discussions. Our work has been supported by the Israel Science Foundation (ISF) and the Directorate for Defense Research and Development (DDR&D)

through Grant No. 3427/21, the ISF grant No. 1113/23, and the US-Israel Binational Science Foundation (BSF) through Grant No. 2020072. A.B. is also supported by the Adams Fellowship Program of the Israel Academy of Sciences and Humanities.

where $\Gamma(s, x)$ is the incomplete gamma function [57]. Plugging into Eq. (26), we find

Appendix A: Calculation of $\Gamma_{k;2n+1}^{\text{FGR}}$

Consider Eq. (26). The integral over ω' evaluates as

$$\int_{\Delta/2}^{\infty} \frac{d\omega'}{\omega'} e^{-\omega'/\omega_c} e^{-i\omega' t} = \Gamma\left(0, \frac{\Delta}{2\omega_c} + \frac{i\Delta t}{2}\right), \quad (\text{A1})$$

$$\Gamma_{k;2n+1}^{\text{FGR}} = 2E_J^2 f_k^2 e^{-\sum_{k'} f_{k'}^2} \sum_{m=0}^{2n+1} \frac{(2z)^{2n+1} \gamma_{1/2}^{2n+1-m}}{(2n+1)!} \binom{2n+1}{m} \int_{-\infty}^{\infty} dt e^{i\omega_k t} \Gamma^m\left(0, \frac{\Delta}{2\omega_c} + \frac{i\Delta t}{2}\right). \quad (\text{A2})$$

The integral over t may be evaluated by choosing a contour that goes around the branch cut of the incomplete gamma function, yielding

$$\int_{-\infty}^{\infty} dt e^{i\omega_k t} \Gamma^m\left(0, \frac{\Delta}{2\omega_c} + \frac{i\Delta t}{2}\right) = \frac{ie^{-\omega_k/\omega_c}}{\Delta/2} \int_0^{\infty} dx e^{-x\omega_k/(\Delta/2)} [(\Gamma(0, -x))^m - (\Gamma(0, -x) + 2\pi i)^m], \quad (\text{A3})$$

where $\Gamma(0, -x) \equiv \Gamma(0, xe^{i\pi-i\delta})$. In order to evaluate the remaining integral analytically, we replace the incomplete gamma function with its series expansions at small and large x , $\Gamma(0, -x) = f(x) - i\pi$, with $f(x \ll 1) \approx -\log x - \gamma$ (where $\gamma \approx 0.5772$ is the Euler-Mascheroni constant), and $f(x \gg 1) \sim -e^x/x$, and find

$$\int_{-\infty}^{\infty} dt e^{i\omega_k t} \Gamma^m\left(0, \frac{\Delta}{2\omega_c} + \frac{i\Delta t}{2}\right) \approx \frac{2e^{-\omega_k/\omega_c}}{\Delta/2} \sum_{l=0}^{\lfloor (m-1)/2 \rfloor} \binom{m}{2l+1} (-1)^l \pi^{2l+1} \int_0^{\infty} dx e^{-x\omega_k/(\Delta/2)} f^{m-2l-1}(x). \quad (\text{A4})$$

Note that the integrand decays at large x provided that $\omega_k > n\Delta$, which is a necessary condition to allow for a $1 \rightarrow 2n+1$ decay process. Indeed, for large enough ω_k/Δ , the integrand decays very rapidly with x , and one may use the expansion of $f(x \ll 1)$, leading to

$$\begin{aligned} & (-1)^{m-2l-1} \int_0^{\infty} dx e^{-x\omega_k/(\Delta/2)} (\log x + \gamma)^{m-2l-1} \\ &= \frac{\Delta/2}{\omega_k} \sum_{r=0}^{m-2l-1} \sum_{p=0}^r \binom{m-2l-1}{r} \binom{r}{p} (-1)^{m+p-1} \gamma^{m-2l-r-1} \Gamma^{(r-p)}(1) \log^p\left(\frac{\omega_k}{\Delta/2}\right), \end{aligned} \quad (\text{A5})$$

where $\Gamma^{(s)}(x)$ is the s derivative of the gamma function. Finally, the exponential factor $e^{-\sum_{k'} f_{k'}^2}$ may also be evaluated analytically using $f_k^2 \approx 2z\Delta e^{-\omega_k/\omega_c}/\omega_k$:

$$e^{-\sum_{k'} f_{k'}^2} \approx \left(\frac{\Delta/2}{\omega_c}\right)^{2z} e^{2z(\gamma-\gamma_{1/2})}. \quad (\text{A6})$$

Plugging everything back into Eq. (A2), we find

$$\begin{aligned} \Gamma_{k;2n+1}^{\text{FGR}}/\Delta &= \frac{2(2z)^{2n+2} E_J^2 e^{-2\omega_k/\omega_c}}{\omega_k^2} \left(\frac{\Delta/2}{\omega_c}\right)^{2z} e^{2z(\gamma-\gamma_{1/2})} \\ &\times \sum_{m=0}^{2n+1} \sum_{l=0}^{\lfloor (m-1)/2 \rfloor} \sum_{r=0}^{m-2l-1} \sum_{p=0}^r \binom{2n+1}{m} \binom{m}{2l+1} \binom{m-2l-1}{r} \binom{r}{p} \frac{1}{(2n+1)!} \\ &\times (-1)^{m+l+p-1} \gamma_{1/2}^{2n+1-m} \gamma^{m-2l-r-1} \pi^{2l+1} \Gamma^{(r-p)}(1) \log^p\left(\frac{\omega_k}{\Delta/2}\right). \end{aligned} \quad (\text{A7})$$

Keeping only the leading logarithmic correction at $\Delta \ll \omega_k \ll \omega_c$ from the sums above is enough to show that the total decay rate, $\Gamma_k^{\text{FGR}} = \sum_{n=1}^{\infty} \Gamma_{k;2n+1}^{\text{FGR}}$, recovers the expected Luttinger-liquid power law: The leading term in Eq. (A7) corresponds to $m = 2n + 1$, $l = 0$, $r = 2n$, and $p = 2n$, and reads (up to the decaying exponential $e^{-2\omega_k/\omega_c}$ and numerical factors that depend on z)

$$\Gamma_{k;2n+1}^{\text{FGR}}/\Delta \sim \frac{E_J^2}{\omega_k^2} \left(\frac{\Delta}{\omega_c}\right)^{2z} \times \frac{(2z)^{2n}}{(2n)!} \log^{2n} \left(\frac{\omega_k}{\Delta/2}\right), \quad (\text{A8})$$

leading to

$$\Gamma_k^{\text{FGR}}/\Delta \sim \frac{E_J^2}{\omega_k^2} \left(\frac{\Delta}{\omega_c}\right)^{2z} \left[\cosh \left(\log \left(\left(\frac{\omega_k}{\Delta/2} \right)^{2z} \right) \right) - 1 \right] \sim E_J^2 \omega_c^{-2z} \omega_k^{2z-2}. \quad (\text{A9})$$

To recover the full numerical prefactor of Γ_k^{FGR} it is necessary to collect all logarithmic corrections of the same order in $\Gamma_k^{\text{FGR}} = \sum_{n=1}^{\infty} \Gamma_{k;2n+1}^{\text{FGR}}$ from the cumbersome expression in Eq. (A7). This is verified numerically in Fig. 3, and easily follows from Eq. (20), since

$$\begin{aligned} \sum_{n=1}^{\infty} \Gamma_{k;2n+1}^{\text{FGR}} &= 2E_J^2 f_k^2 e^{-\sum_{k'} f_{k'}^2} \int_{-\infty}^{\infty} dt e^{i\omega_k t} \sum_{n=1}^{\infty} \frac{1}{(2n+1)!} \left[\sum_{k'} f_{k'}^2 e^{-i\omega_{k'} t} \right]^{2n+1} \\ &= 2E_J^2 f_k^2 e^{-\sum_{k'} f_{k'}^2} \int_{-\infty}^{\infty} dt e^{i\omega_k t} \left[\sinh \left(\sum_{k'} f_{k'}^2 e^{-i\omega_{k'} t} \right) - 1 \right] \\ &\approx E_J^2 f_k^2 \int_{-\infty}^{\infty} dt e^{i\omega_k t} \exp \left(- \sum_{k'} f_{k'}^2 (1 - e^{-i\omega_{k'} t}) \right), \end{aligned} \quad (\text{A10})$$

where, going from the second to the third line above, we used $e^{-\sum_{k'} f_{k'}^2} \sim \Delta^{2z}$ to discard terms that vanish in the thermodynamic limit. We thus recover the total decay rate in the thermodynamic limit, which was evaluated in Ref. [31].

Appendix B: Details of numerical evaluation of the decay rates

1. Average over disorder

As mentioned above, one must keep a finite plasma frequency in order to break the massive degeneracy of the many-body modes. This degeneracy is further avoided by introducing some disorder that is always present in any experimental setup, due to deviations in the values of the array Josephson couplings and capacitances. We assume a realistic deviation of $\pm 10\%$ around the nominal values of the line parameters $E_J^{\text{line}}, C^{\text{line}}, C_g$ in Eq. (12), and, for each realization, find the modes by solving the corresponding generalized eigenvalue problem numerically. An example for the modes of 1-, 3-, and 5-photon states for a single realization of disorder is shown in Fig. 1. In the calculation of the dressed propagators, we use each realization of modes to calculate the propagators of the modes iteratively, going up from the low-frequency modes. The spectral functions measured in an experiment correspond to single realizations of disorder, as the ones displayed in

Figs. 4 and 5. The decay rates shown in Fig. 4 are averaged over 50 realizations of disorder.

2. Renormalization group considerations at low frequencies

In Figs. 4 and 5, we use $z = 1/2$. Note that since $z < 1$, the boundary cosine operator $\mathcal{H}_I = E_J \cos \phi_0$ is relevant in an RG sense and cannot be treated as a perturbation below the RG scale $E_J^* = (E_J/\omega_c^z)^{1/(1-z)}$. Using our choice of numerical parameters, we find $E_J^*/\Delta < 1$ at $N = 10^4$ (and smaller at smaller array sizes), such that our perturbative analysis is valid from the very first mode. Note that in principle, if the RG scale were larger with several array modes below it, it would have been possible to extend our treatment to these low-frequency modes as well by expanding around the strong-coupling fixed-point. A strong-coupling expansion should lead to the same structure of the self-energy, but with new f_k factors. It is then possible to stitch together the two regimes, by using the f_k factors from the strong-coupling expansion at frequencies below E_J^* , and the perturbative f_k at frequencies above E_J^* .

[1] P. A. M. Dirac and N. H. D. Bohr, The quantum theory of the emission and absorption of radiation, *Proceedings*

of the Royal Society of London. Series A, Containing Pa-

- pers of a Mathematical and Physical Character **114**, 243 (1997).
- [2] E. Fermi, *Nuclear Physics: A Course Given by Enrico Fermi at the University of Chicago* (University of Chicago Press, 1950).
 - [3] G. C. Stey and R. W. Gibberd, Decay of quantum states in some exactly soluble models, *Physica* **60**, 1 (1972).
 - [4] J. H. Eberly, N. B. Narozhny, and J. J. Sanchez-Mondragon, Periodic Spontaneous Collapse and Revival in a Simple Quantum Model, *Physical Review Letters* **44**, 1323 (1980).
 - [5] P. W. Milonni, J. R. Ackerhalt, H. W. Galbraith, and M.-L. Shih, Exponential decay, recurrences, and quantum-mechanical spreading in a quasicontinuum model, *Physical Review A* **28**, 32 (1983).
 - [6] J. M. Zhang and Y. Liu, Fermi's golden rule: its derivation and breakdown by an ideal model, *European Journal of Physics* **37**, 065406 (2016).
 - [7] N. G. Kelkar, M. Nowakowski, and K. P. Khemchandani, Hidden evidence of nonexponential nuclear decay, *Physical Review C* **70**, 024601 (2004).
 - [8] C. Rothe, S. I. Hintschich, and A. P. Monkman, Violation of the Exponential-Decay Law at Long Times, *Physical Review Letters* **96**, 163601 (2006).
 - [9] Y. A. Litvinov, F. Bosch, N. Winckler, D. Boutin, H. G. Essel, T. Faestermann, H. Geissel, S. Hess, P. Kienle, R. Knöbel, C. Kozhuharov, J. Kurcewicz, L. Maier, K. Beckert, P. Beller, C. Brandau, L. Chen, C. Dimopoulou, B. Fabian, A. Fragner, E. Haettner, M. Hausmann, S. A. Litvinov, M. Mazzocco, F. Montes, A. Musumarra, C. Nociforo, F. Nolden, W. Plaß, A. Prochazka, R. Reda, R. Reuschl, C. Scheidenberger, M. Steck, T. Stöhlker, S. Torilov, M. Trassinelli, B. Sun, H. Weick, and M. Winkler, Observation of non-exponential orbital electron capture decays of hydrogen-like 140Pr and 142Pm ions, *Physics Letters B* **664**, 162 (2008).
 - [10] G. Andersson, B. Suri, L. Guo, T. Aref, and P. Delsing, Non-exponential decay of a giant artificial atom, *Nature Physics* **15**, 1123 (2019).
 - [11] T. Micklitz, A. Morningstar, A. Altland, and D. A. Huse, Emergence of Fermi's Golden Rule, *Physical Review Letters* **129**, 140402 (2022).
 - [12] B. L. Altshuler, Y. Gefen, A. Kamenev, and L. S. Levitov, Quasiparticle Lifetime in a Finite System: A Nonperturbative Approach, *Physical Review Letters* **78**, 2803 (1997).
 - [13] D. M. Basko, I. L. Aleiner, and B. L. Altshuler, Metal-insulator transition in a weakly interacting many-electron system with localized single-particle states, *Annals of Physics* **321**, 1126 (2006).
 - [14] L. D'Alessio, Y. Kafri, A. Polkovnikov, and M. Rigol, From quantum chaos and eigenstate thermalization to statistical mechanics and thermodynamics, *Advances in Physics* **65**, 239 (2016).
 - [15] D. A. Abanin, E. Altman, I. Bloch, and M. Serbyn, Colloquium: Many-body localization, thermalization, and entanglement, *Reviews of Modern Physics* **91**, 021001 (2019).
 - [16] K. Seetharam, P. Titum, M. Kolodrubetz, and G. Refael, Absence of thermalization in finite isolated interacting Floquet systems, *Physical Review B* **97**, 014311 (2018).
 - [17] A. Morningstar, D. A. Huse, and V. Khemani, Universality classes of thermalization for mesoscopic Floquet systems, *Physical Review B* **108**, 174303 (2023).
 - [18] M. Žnidarič, Weak Integrability Breaking: Chaos with Integrability Signature in Coherent Diffusion, *Physical Review Letters* **125**, 180605 (2020).
 - [19] M. Brenes, T. LeBlond, J. Goold, and M. Rigol, Eigenstate Thermalization in a Locally Perturbed Integrable System, *Physical Review Letters* **125**, 070605 (2020).
 - [20] V. B. Bulchandani, D. A. Huse, and S. Gopalakrishnan, Onset of many-body quantum chaos due to breaking integrability, *Physical Review B* **105**, 214308 (2022).
 - [21] H. Bernien, S. Schwartz, A. Keesling, H. Levine, A. Omran, H. Pichler, S. Choi, A. S. Zibrov, M. Endres, M. Greiner, V. Vuletić, and M. D. Lukin, Probing many-body dynamics on a 51-atom quantum simulator, *Nature* **551**, 579 (2017).
 - [22] R. Kuzmin, N. Grabon, N. Mehta, A. Burshtein, M. Goldstein, M. Houzet, L. Glazman, and V. Manucharyan, Inelastic Scattering of a Photon by a Quantum Phase Slip, *Physical Review Letters* **126**, 197701 (2021).
 - [23] R. Kuzmin, N. Mehta, N. Grabon, R. Mencia, and V. E. Manucharyan, Superstrong coupling in circuit quantum electrodynamics, *npj Quantum Information* **5**, 1 (2019).
 - [24] J. Puertas Martínez, S. Léger, N. Gheeraert, R. Dassonneville, L. Planat, F. Foroughi, Y. Krupko, O. Buisson, C. Naud, W. Hasch-Guichard, S. Florens, I. Snyman, and N. Roch, A tunable Josephson platform to explore many-body quantum optics in circuit-QED, *npj Quantum Information* **5**, 1 (2019).
 - [25] K. Le Hur, Kondo resonance of a microwave photon, *Physical Review B* **85**, 140506 (2012).
 - [26] M. Goldstein, M. H. Devoret, M. Houzet, and L. I. Glazman, Inelastic Microwave Photon Scattering off a Quantum Impurity in a Josephson-Junction Array, *Physical Review Letters* **110**, 017002 (2013).
 - [27] N. Gheeraert, X. H. H. Zhang, T. Sépulcre, S. Bera, N. Roch, H. U. Baranger, and S. Florens, Particle production in ultrastrong-coupling waveguide QED, *Physical Review A* **98**, 043816 (2018).
 - [28] M. Houzet and L. Glazman, Critical Fluorescence of a Transmon at the Schmid Transition, *Physical Review Letters* **125**, 267701 (2020).
 - [29] A. Burshtein, R. Kuzmin, V. E. Manucharyan, and M. Goldstein, Photon-Instanton Collider Implemented by a Superconducting Circuit, *Physical Review Letters* **126**, 137701 (2021).
 - [30] S. Léger, T. Sépulcre, D. Fraudet, O. Buisson, C. Naud, W. Hasch-Guichard, S. Florens, I. Snyman, D. M. Basko, and N. Roch, Revealing the finite-frequency response of a bosonic quantum impurity, *SciPost Physics* **14**, 130 (2023).
 - [31] R. Kuzmin, N. Mehta, N. Grabon, R. A. Mencia, A. Burshtein, M. Goldstein, and V. E. Manucharyan, Observation of the schmid-bulgadaev dissipative quantum phase transition, *Nature Physics* **21**, 132 (2025).
 - [32] A. Burshtein and M. Goldstein, Inelastic Decay from Integrability, *PRX Quantum* **5**, 020323 (2024).
 - [33] M. Houzet, T. Yamamoto, and L. I. Glazman, Microwave spectroscopy of the Schmid transition, *Physical Review B* **109**, 155431 (2024).
 - [34] B. Remez, V. D. Kurilovich, M. Rieger, and L. I. Glazman, Bloch oscillations in a transmon embedded in a resonant electromagnetic environment, *Phys. Rev. B* **110**, 054508 (2024).

- [35] A. Burshtein, D. Shuliutsky, R. Kuzmin, V. E. Manucharyan, and M. Goldstein, [Numerical evaluation of the real-time photon-instanton cross-section in a superconducting circuit](#) (2024), arXiv:2410.23062 [quant-ph].
- [36] N. Mehta, R. Kuzmin, C. Ciuti, and V. E. Manucharyan, Down-conversion of a single photon as a probe of many-body localization, [Nature](#) **613**, 650 (2023).
- [37] D. Fraudet, I. Snyman, D. M. Basko, S. Léger, T. Sépulcre, A. Ranadive, G. Le Gal, A. Torras-Coloma, W. Guichard, S. Florens, and N. Roch, Direct detection of down-converted photons spontaneously produced at a single josephson junction, [Phys. Rev. Lett.](#) **134**, 013804 (2025).
- [38] L. Giacomelli and C. Ciuti, Emergent quantum phase transition of a Josephson junction coupled to a high-impedance multimode resonator, [Nature Communications](#) **15**, 5455 (2024).
- [39] A. Schmid, Diffusion and Localization in a Dissipative Quantum System, [Physical Review Letters](#) **51**, 1506 (1983).
- [40] S. Bulgadaev, Phase diagram of a dissipative quantum system, *ZhETF Pisma Redaktsiiu* (1984).
- [41] F. Borletto, L. Giacomelli, and C. Ciuti, Circuit quantum electrodynamics of direct and dual shapiro steps with finite-size-transmission-line resonators, [Phys. Rev. Appl.](#) **22**, 054061 (2024).
- [42] N. Mehta, C. Ciuti, R. Kuzmin, and V. E. Manucharyan, [Theory of strong down-conversion in multi-mode cavity and circuit QED](#) (2022), arXiv:2210.14681 [cond-mat, physics:quant-ph].
- [43] V. E. Manucharyan, J. Koch, L. I. Glazman, and M. H. Devoret, Fluxonium: Single Cooper-Pair Circuit Free of Charge Offsets, [Science](#) **326**, 113 (2009).
- [44] R. Kuzmin, R. Mencia, N. Grabon, N. Mehta, Y.-H. Lin, and V. E. Manucharyan, Quantum electrodynamics of a superconductor–insulator phase transition, [Nature Physics](#) **15**, 930 (2019).
- [45] M. Bard, I. V. Protopopov, and A. D. Mirlin, Decay of plasmonic waves in Josephson junction chains, [Physical Review B](#) **98**, 224513 (2018).
- [46] H.-K. Wu and J. D. Sau, Theory of coherent phase modes in insulating Josephson junction chains, [Physical Review B](#) **99**, 214509 (2019).
- [47] M. Houzet and L. I. Glazman, Microwave Spectroscopy of a Weakly Pinned Charge Density Wave in a Superconductor, [Physical Review Letters](#) **122**, 237701 (2019).
- [48] R. Lefebvre and J. Savolainen, Memory functions and recurrences in intramolecular processes, [The Journal of Chemical Physics](#) **60**, 2509 (1974).
- [49] J. M. Martinis, M. Ansmann, and J. Aumentado, Energy decay in superconducting josephson-junction qubits from nonequilibrium quasiparticle excitations, [Phys. Rev. Lett.](#) **103**, 097002 (2009).
- [50] J. M. Martinis, K. B. Cooper, R. McDermott, M. Steffen, M. Ansmann, K. D. Osborn, K. Cicak, S. Oh, D. P. Pappas, R. W. Simmonds, and C. C. Yu, Decoherence in josephson qubits from dielectric loss, [Phys. Rev. Lett.](#) **95**, 210503 (2005).
- [51] A. O. Gogolin, A. A. Nersesyan, and A. M. Tsvelik, *Bosonization and Strongly Correlated Systems* (Cambridge University Press, 2004).
- [52] P. J. D. Crowley and A. Chandran, Mean-field theory of failed thermalizing avalanches, [Phys. Rev. B](#) **106**, 184208 (2022).
- [53] J. P. Pekola and B. Karimi, Quantum thermalization via multiwave mixing, [Phys. Rev. Res.](#) **6**, L042023 (2024).
- [54] S. Ghoshal and A. Zamolodchikov, Boundary s matrix and boundary state in two-dimensional integrable quantum field theory, [International Journal of Modern Physics A](#) **09**, 3841 (1994).
- [55] M. Rigol, V. Dunjko, V. Yurovsky, and M. Olshanii, Relaxation in a Completely Integrable Many-Body Quantum System: An Ab Initio Study of the Dynamics of the Highly Excited States of 1D Lattice Hard-Core Bosons, [Physical Review Letters](#) **98**, 050405 (2007).
- [56] A. Burshtein and M. Goldstein, Quantum simulation of the microscopic to macroscopic crossover using superconducting quantum impurities, [10.5281/zenodo.15319197](#) (2025).
- [57] M. Abramowitz and I. A. Stegun, *Handbook of Mathematical Functions: With Formulas, Graphs, and Mathematical Tables* (Courier Corporation, 1965).